Unprecedented intramolecular pancake bonding in a {Dy_2} single-molecule magnet

Maykon A. Lemes,[a] Niki Mavragani,[a] Paul Richardson,[a] Yixin Zhang,[a] Bulat Gabidullin,[a] Jaclyn L. Brusso,[a*] Jani O. Moilanen,[b*]and Muralee Murugesu[a*]

The first example of unique coordination induced intramolecular pancake bonding was achieved through the reduction of two bis(pyrazolyl)-tetrazine ligands, affording [M^{III}_2(μ-(bpytz)$_2$)(THMD)$_4$](M = Dy, Y; bpytz = 3,6-bis(3,5-dimethyl-pyrazolyl)-1,2,4,5-tetrazine; TMHD = 2,2,6,6-tetramethyl-3,5-heptanedionate). To provide a cohesive magneto-structural correlation, the mono bis(pyrazolyl)-tetrazine bridged congener [Dy^{III}_2(μ-bpytz)(THMD)$_6$]·4(C_6H_6) was also isolated. Both metal complexes exhibit single-molecule magnet behaviour under an applied dc field.

Radicals have long been considered transient, highly reactive species; however, in recent years a number of stable radical based systems have been reported.[1] Although many have been shown to be stable in the solid state, a number are still susceptible to self-association (i.e., dimerization). While dimerization can be suppressed through sterics, the increased bulkiness around the radical centre unfortunately inhibits close proximity of the unpaired spins, thereby inhibiting potential conductive and/or magnetic properties of the resulting materials. Alternatively, coordination chemistry can be employed as a useful route to prevent dimerization, and has been widely exploited in recent years due to the potential of such systems in applications ranging from catalysis to molecular magnetism.[2] In the case of the latter, research on single-molecule magnets (SMMs) has recently focused on the use of radicals as ligands to enhance the magnetic properties of SMMs through the exchange coupling of the radical- and metal-based spins.[3] SMMs are defined as molecules that retain the slow relaxation of their magnetization upon removal of an applied field, acting as magnets below blocking temperatures.[4] The strong interaction between the spin of the radical with the unpaired electrons of a metal ion effectively suppresses the quantum tunneling of the magnetization and fast spin relaxation pathways involving spin excited states, thus promoting a thermal relaxation pathway for magnetization reversal.[3b] If radicals are used as bridging units between two or more metal centres, then magnetic communication between the metal ions can be enhanced.[2c,3b-c] As such, lanthanide based SMMs containing bridging, spin-bearing ligands have attracted considerable attention. Currently, the best performing polynuclear SMM is a dinuclear metal complex containing a dinitrogen radical bridge with a blocking temperature of 20 K and giant coercive field of H_c = 7.9 T at 10 K.[3c] While this validates the design strategy, the presence of the dinitrogen radical bridge imparts air sensitivity to the molecule. Nonetheless, this represents an excellent example in which metal coordination stabilizes an otherwise unisolable radical.

Although self-association of radicals can be inhibited thanks to the coordination environment dictated by the geometry of the metal ion, employing bridging radical ligands remains an ongoing challenge. This is due in large part to the access of stable delocalized radicals that can impart efficient magnetic exchange between two or more metal ions.[2c] To that end, tetrazine based ligands offer multiple coordination pockets, while the nitrogen content and delocalized nature of the π-system enhance the stability towards oxygen.[5] Thanks to the relatively small energy difference between the π and π* molecular orbitals, tetrazine moieties can be easily reduced at low reduction potential.[5i] These features have been demonstrated using transition metals[5a,b,h,2d] as well as a few examples employing lanthanide ions.[5k,22a]

As mentioned, metal coordination is highly effective in the quest to prevent dimerization; however, π-dimerization achieved through metal coordination is considerably less explored. The only example reported to date is the formation of a π-dimer attained by appending two radical moieties on the cyclopentadienyl rings of ferrocene, as elegantly demonstrated by Hicks *et al*.[6] While this represents an intramolecular π-dimer associated with a metal complex, these π-dimers are not directly bound to the metal ion. To date, coordination induced π-dimerization or examples of bridging π-dimers between two metal ions have yet to be reported. This is likely due to the change in electron density of the radical and coupling of the radical and metal spins upon coordination, thereby decreasing the stabilization effect of dimerization. Furthermore, coordination to a metal centre dictates the sterics and orientation of the radical moiety and its proximity to neighbouring radicals. All of these properties inhibit

[a] *Department of Chemistry and Biomolecular Sciences. University of Ottawa, ON, Canada K1N 6N5. Email: m.murugesu@uottawa.ca; Tel: + (613) 562 5800 ext. 2733.*

[b] *Department of Chemistry, Nanoscience Centre, P.O. Box 35, FI-40014, University of Jyväskylä, Finland*

† Electronic Supplementary Information (ESI) available: Experimental details, crystallographic data, EPR analysis, magnetic studies and computational data. CCDC1858838, 1858840 and 1976893. See DOI: 10.1039/x0xx00000x

intramolecular dimerization and minimize the tendency for intermolecular self-association between neighbouring radicals.

To that end, herein we report an unprecedented intramolecular π-π stacking interaction, also called a pancake bond, in a {Dy_2} single-molecule magnet by utilizing a bis(pyrazolyl)-tetrazine based ligand framework. More specifically, the synthesis, extensive computational studies and detailed magnetic analysis of two structurally related dinuclear Dy^{III} SMMs, revealed through an applied dc field, are presented; a dinuclear Dy^{III} metal complex [Dy^{III}_2(μ-bpytz)(THMD)$_6$]·4(C_6H_6) (**1**·4C_6H_6; where bpytz = 3,6-bis(3,5-dimethyl-pyrazolyl)-1,2,4,5-tetrazine; TMHD = 2,2,6,6-tetramethyl-3,5-heptanedionate) with a neutral tetrazine bridging ligand, alongside [Dy^{III}_2(μ-(bpytz)$_2$)(THMD)$_4$] (**2**), a dinuclear compound containing a unique π-dimerized tetrazine bridge. The yttrium analogue [Y^{III}_2(μ-(bpytz)$_2$)(THMD)$_4$] (**3**), which is isostructural to **2**, was also prepared and studied to confirm the diamagnetic nature of the bridging π-dimer ligand. This report represents the first example of a coordination induced tetrazine intramolecular π-dimer contained within a single molecule.

Preparation of compounds **1**·4C_6H_6, **2** and **3** follow similar procedures, beginning with the reaction of one equivalent of bpytz with one equivalent of M(TMHD)$_3$ (where M = Dy or Y) in benzene under aerobic conditions, which affords a dark brown solution (for **1**·4C_6H_6, see ESI for more details). Upon vapour diffusion of the aforementioned solution with acetonitrile (CH_3CN), red block-like single crystals of [Dy^{III}_2(μ-bpytz)(THMD)$_6$]·4C_6H_6 (**1**·4C_6H_6) suitable for single crystal X-ray diffraction (SCXRD) were obtained in 85% yield (Scheme 1). The same product can be isolated if the reaction is performed under anaerobic conditions (**2** and **3**), whereas a dark green solution is obtained if the reaction is carried out in the presence of one equivalent of cobaltocene ($CoCp_2$). Slow diffusion of CH_3CN into the latter yields dark green block-like crystals of **2** in 80% yield. Alternatively, compound **2** can be prepared from the reaction of **1**·4C_6H_6 with $CoCp_2$ in the same solvolitic conditions, though we found this resulted in lower yield percentages. This may be attributed to the sacrificial nature of the reaction. It is noteworthy that attempts to isolate the mono-radical anion bridged dinuclear {Dy_2} compound were unsuccessful, as were attempts to prepare the radical anion or π-dimer of bpytz in the absence of metal ions. Interestingly, compounds **1**·4C_6H_6, **2**, and **3** exhibit solid-state air-stability over long periods of time, as observed *via* infrared (IR) measurements. For example, under aerobic conditions over a period of 20 days, no change was observed in the IR spectra of **2** (Fig. S1).

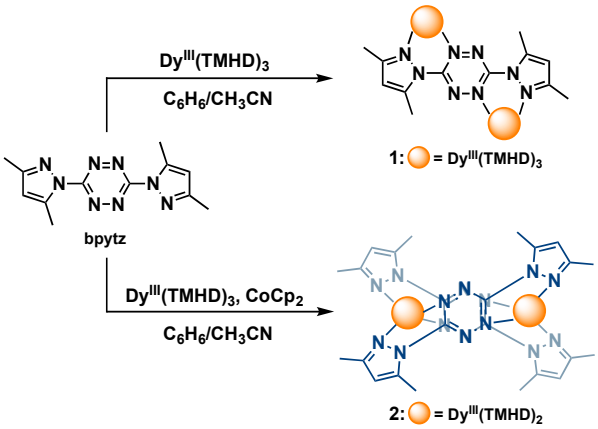

Scheme 1 Synthetic route for the isolation of **1**·4(C_6H_6) and **2**, where bpytz = 3,6-bis(3,5-dimethyl-pyrazolyl)-1,2,4,5-tetrazine and TMHD = 2,2,6,6-tetramethyl-3,5-heptanedionate. The dark blue *vs.* lighter blue bpytz in **2** indicates the above and below arrangement of the reduced ligand π-dimer.

Single-crystal X-ray diffraction analysis reveals that **1**·4C_6H_6 and **2** crystallize in the triclinic $P\bar{1}$ and trigonal $P3_221$ space groups, respectively. The molecular structures of both metal complexes are shown in Fig. 1 and Fig. S2-S4, and X-ray data along with selected distances and angles are given in Tables S1-S3. In **1**·4C_6H_6, the centrosymmetric dinuclear metal complex is composed of two Dy^{III} ions bridged by a neutral bpytz ligand; close inspection of the N-N distance (1.32(5) Å) in the tetrazine core is in good agreement with that of the free ligand, thus corroborating the neutral form of the tetrazine moiety. Three TMHD ligands complete the coordination environment around each metal centre, affording square antiprismatic geometry as confirmed by SHAPE analysis (Table S4).[7] The two metal ions are coordinated in a bidentate fashion in the bipy-like coordination pocket of the bpytz ligand with intramolecular Dy···Dy distances of 8.01(4)Å. Four benzene solvent molecules are also present in the crystal lattice.

In the case of **2**, the centrosymmetric compound is comprised of two Dy^{III} ions bridged by two bpytz ligands, with two TMHD coordinated to each metal centre thereby affording a geometry that can best be described as square antiprism (SHAPE analysis, Table S4).[7] Here, the four TMHD co-ligands contribute a total charge of 4–, therefore the additional charge to stabilize the 6+ metal ions must be provided by two reduced bpytz ligands with each having a charge of 1–. Reduction of the bpytz ligands in **2** is thus supported by charge balance considerations. The crystallographic changes observed in the tetrazine core through elongation of the azo N-N distances from 1.32(5) Å to 1.39(6)Å further endorse the negative charge on the tetrazine moieties.[5] The assembly of the two bpytz ligands allows the tetrazine rings to face each other at a distance of 2.73(5) Å (Fig. S3 and S4); a distance considerably longer than a single bond (ca. 1.43 – 1.54 Å) yet notably shorter than the sum of the van der Waals radii (ca. 3.0 – 3.4 Å).[8] The packing arrangement displays intermolecular Dy···Dy distances of 12.11(1)Å, while the Dy···Dy intramolecular distance is 7.10(8)Å.

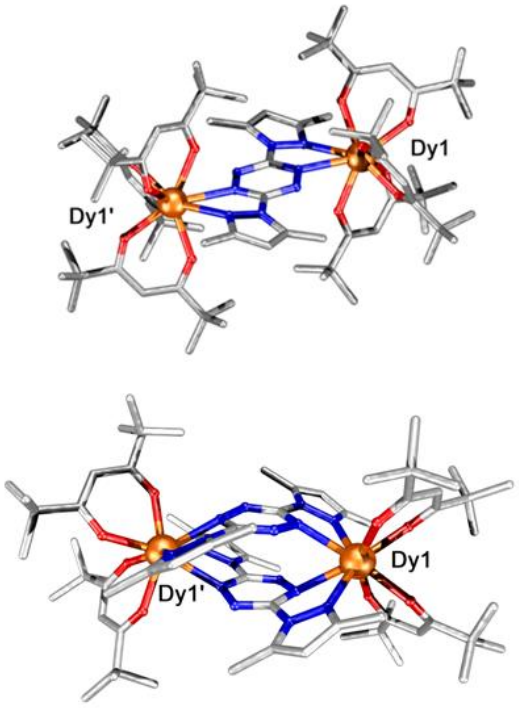

Fig. 1 Molecular structure of **1** (top) and **2** (bottom). Solvent molecules and hydrogen atoms were omitted for clarity. Color code: Dy (orange), C (gray), N (blue), O (red).

Although reduction of tetrazine in coordination metal complexes is known to afford tetrazinyl radicals,[5] here the observed air-stability, close intramolecular contacts and magnetic data (*vide infra*) indicate spin pairing of the tetrazinyl moieties within the molecule. Despite the electrostatic repulsion expected between charged radical species, examples of π-dimerized radical cations are known as are radical anions, however, there are fewer examples of the latter (e.g., TCNE and TCNQ).[9] While π-dimerization is quite common among organic radicals, it is rare in coordination metal complexes and, when present, tends to lead to extended coordination networks.[10] In **2**, we have a π-dimer that acts as an intramolecular bridge between two metal centres in a discrete coordination compound. Here the charge imparted by the cationic lanthanide ions likely alleviate some of the electrostatic repulsion between the radical anions, facilitating the formation of the π-dimerized bridging ligand and perhaps stabilizing self-association. The interaction between the bpytz ligands in **2**, which can be referred to as pancake bonding (i.e., multicentered 2-electron bonding; mc-2e),[11] is unique to this molecule and such features have yet to be reported.

In an effort to validate the diamagnetic nature of the bridging ligand in **2**, the yttrium analogue **3** was synthesized following a similar procedure. SCXRD analysis of **3** reveals that it crystallizes in thetrigonal $P3_221$ space group and is isostructural with **2**, as evidence by the structural overlay (Fig. S5), infrared spectroscopy (Fig. S6) and powder X-ray diffraction patterns (Fig. S7). Solid state magnetic studies on **3** reveal its diamagnetic nature, supporting spin pairing of the two reduced bpytz moieties and hence π-dimerization of the bridging ligand. Solution electron paramagnetic resonance (EPR) studies were also carried out on **3**, which exhibit a nine-line pattern signal attributed to a single bpytz radical anion (i.e., simulated using a model based on hyperfine coupling of four equivalent ^{14}N nuclei with a_N = 0.507 mT; Fig. S8). However, such signals must be taken with caution as **3** is sparingly soluble in common organic solvents and, under these conditions, its stability is limited; attempts to probe this interaction through NMR experiments were inconclusive. As such, the obtained signal is likely arising from the dissociated compound in solution. Moreover, a half-field signal arising from the population of the triplet state was not observed in the EPR studies, indicative of strong antiferromagnetic coupling between the two bpytz radical anions.

To further analyse the nature of the pancake bond within compound **2**, broken symmetry density functional theory (BS-DFT)[12] and complete active space self-consistent field (CASSCF) calculations[13] were first carried out for **3** and its simplified model system $[Y_2^{III}(\mu\text{-(bpytz)}_2)(PD)_4]$ (**4**; where PD = propanedionate) using the coordinates adapted from the crystal structure of **3** and only optimizing the positions of the hydrogen atoms (see computational details in the ESI included in Fig. S9). Two spin bearing radicals that strongly interact can form a triplet or singlet state system depending on the ferromagnetic (FM) or antiferromagnetic (AFM) coupling of their spins, respectively. In the case of a pancake bonded system, the ground state is typically a singlet.[12e] Here, the singlet state is favoured over a triplet one, because the in-phase components of identical singly occupied molecular orbitals (SOMOs) of the radicals that form the pancake bond strongly overlap with each other. The overlap of in-phase components of identical SOMOs leads to a covalent type interaction between two radicals that automatically favours an AFM interaction.[12e,14a]

The wave function of the singlet state pancake bonded system usually contains a considerable amount of singlet diradical character.[12e] The singlet diradical is a molecular entity in which two electrons occupy two (nearly) degenerate molecular orbitals.[15] The wave function of such a system is multiconfigurational and cannot be described by the single Slater determinant methods such as the restricted Hartree-Fock theory. Therefore, multiconfigurational approaches like the CASSCF are needed. In a strict sense, the basic formalism of DFT is also a single determinant approach but it is able to treat small to moderate amounts of the singlet diradical character. Because of this, it is an applicable computational method to model the pancake bond within compounds **3** and **4**. To confirm the ground state multiplicity of **3** and **4**, we first calculated the vertical singlet-triplet gap (VSTG) for **4** using a variety of different exchange-correlation functionals and the Yamaguchi projection.[16] Depending on the functional used, BS-DFT calculations predicted the triplet state to be ~ 3250–4000 cm^{-1} higher in energy than the singlet state (Table S5). The validity of the small model system **4** was confirmed by calculating the VSTG for **3** using the LC-ωPBE-D3/def2-TZVP level of

theory[17a-c,18]; very similar values were obtained for **3** (-3228 cm^{-1}) and **4** (-3249 cm^{-1}). Small geometrical changes can influence the value of the STG and it is very likely that **3** does not adopt the same geometry in the solution and solid state. Thus, we also calculated the adiabatic singlet-triplet gaps (ASTG) for the gas-phase optimized geometries of **3** and **4** (only at the LC-ωPBE-D3 level for **3**) using the same exchange-correlation functionals as for the VSTG.[14] Geometry optimizations of the HS and LS states of **3** and **4** revealed that the intramolecular centroid-centroid (Cnt-Cnt) ring distance of two interacting $bpytz^{\bullet-}$ radicals for the gas-phase optimized structures are ~0.1–0.3 Å longer than the intramolecular Cnt-Cnt ring distance of the crystal structure of **3** (Table S6). The best agreement between experimental and calculated Cnt-Cnt distance is obtained with the B3LYP-D3/def2-TZVP,[17d-f,18] PBE1PBE-D3/def2-TZVP,[17g,h,18] and LC-ωPBE-D3/def2-TZVP[17a-c,18] levels of theory that predict the calculated Cnt-Cnt distance of the ground LS state to be only ~0.1 Å longer than the experimental value. Although different projections were used to obtain the VSTGs and ASTGs, it is evident from the calculated data that the small increase in the Cnt-Cnt distance has effect on the calculated singlet-triplet gaps of **3** and **4**; the ASTGs are smaller (~-1780 to -2600 cm^{-1}) than the VSTGs (~ -3250 to -4000 cm^{-1}) (Tables S5 and S7). Nevertheless, such high STGs very likely explain why the thermally accessible triplet state is not populated even at the room temperature, as supported by EPR analysis. Moreover, the calculated VSTGs and ASTGs fully confirm that the ground state of **3** and **4** is a singlet state.

The highest occupied molecular orbital (HOMO) and lowest unoccupied molecular orbital (LUMO) obtained at the LC-ωPBE-D3/def2-TZVP level of theory for the singlet state of **4** are shown in Fig. 2. As can be seen, the $bpytz^{\bullet-}$ radicals within the metal complex are π-dimerized through an orbital interaction that resembles covalent-type bonding. The spin density distribution is also presented in Fig. 2, revealing a strong localization of spin density on the central rings of the two $bpytz^{\bullet-}$, as well as (almost) equal distribution for α and β spin density. To quantify this orbital interaction in **3** and **4**, we calculated the vertical and adiabatic rad-rad coupling constant ($J_{rad\text{-}rad}$) using the Yamaguchi and adiabatic projections, respectively, and BS-DFT formalism.[14,16] We evaluated the singlet diradical character, unpaired electron density,[19] and formal bond order (p_{NO})[20] of **4** utilizing natural orbital occupation numbers (NOONs) from the CASSCF calculations (see ESI for details). The CASSCF calculations were performed for the frozen and LC-ωPBE-D3/def2-TZVP optimized ground state gas-phase geometry of **4**. Since the $J_{rad\text{-}rad}$ equals the vertical and adiabatic singlet-triplet gaps (see above), the calculated $J_{rad\text{-}rad}$ values indicate a strong antiferromagnetic interaction between two $bpytz^{\bullet-}$ in **3** and **4** (Tables S5 and S7). These values of $J_{rad\text{-}rad}$ are in line with values reported for other strongly π-dimerized radical systems.[14a]

NOONs are the eigenvalues of the one-particle electron density matrix, and they converge towards values that they adopt in the exact wave function when the level of theory used is high enough.[21] Because of this, NOONs at the CASSCF level of theory can be used as a benchmark of the singlet diradical character; in a perfect diradical, two natural orbitals are each occupied exactly by one electron. Thus, a suitable index for diradical character is obtained by comparing the occupation number of the acceptor orbital n_{ACC} (formally the LUMO in the case of **4**) to the reference value of one electron (n_{ACC} /1.00) × 100%. Despite the size of active space and the geometry employed (i.e., crystal structure or gas-phase optimized), the investigation of NOONs reveals that ~0.4–0.6 electrons are transferred from the formally HOMO to LUMO, which corresponds to 40–60 % of the singlet diradical character (Tables S8 and S9). Only a small amount of electron density is distributed from the other formally occupied π-orbitals to unoccupied π-orbitals that all have relatively small NOONs.

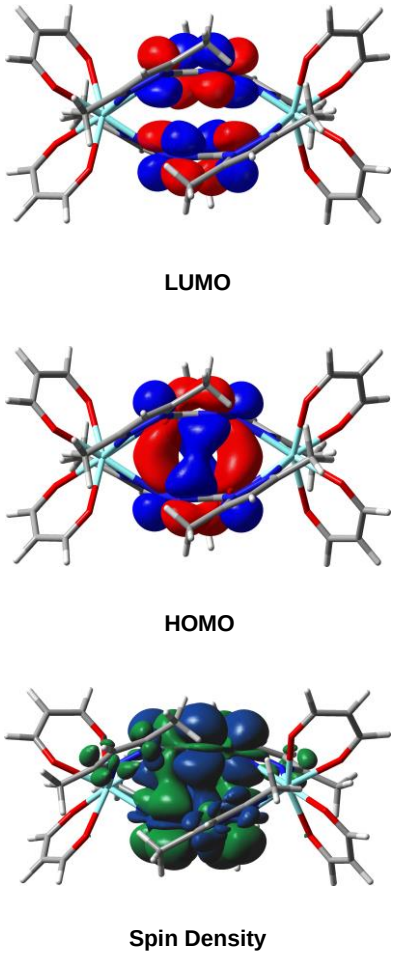

Fig. 2 Lowest occupied molecular orbital (LUMO; top) and highest occupied molecular orbital (HOMO; middle), as well as the spin density distribution (bottom; blue = α spin density; green = β spin density) for **4**. Similar HOMO, LUMO and spin density distributions are observed for **3**.

The results indicate that the wave function of **4** contains a notable amount of the singlet diradical character, and the formally HOMO and LUMO contribute most to the formation of the pancake bond between π-dimerized $bpytz^{\bullet-}$ radicals. NOONs can be also used to evaluate the p_{NO} and unpaired

electron density between bpytz$^{\bullet-}$ radicals, with the latter measuring the separation of an electron pair into different spatial regions.[19] By using the occupation numbers of the frontier natural orbitals (formally the HOMO and LUMO) of **4** from the CASSCF calculations, the p_{NO} value of ~0.4–0.6 is obtained for the frozen and optimized geometry of **4**. The unpaired electron density is measured by calculating the total number of effectively unpaired electrons (N_u) between bpytz$^{\bullet-}$ ligands. The calculated value of N_u for **4** deviates between 0.74 and 1.36 for the crystal structure geometry and 1.07 and 1.41 for the gas-phase optimized, depending on the size of active space used in the CASSCF calculations. Most importantly, such high values reflect the notably diradical character of compound **4** (Tables S10 and 11). Both the p_{NO} and N_u values obtained for **4** are in a good agreement with values reported for other systems containing a single pancake bond.[20,22] Overall, these calculations indicate that the interaction between the bpytz moieties resembles a covalent bond rather than a weak AFM exchange interaction. In this respect, the π-dimerized bpytz$^{\bullet-}$ radicals should function as a diamagnetic linker between the two Dy^{III} ions within **2**.

To validate the nature of the intramolecular π-dimerized bridging ligand and to probe the static and dynamic magnetic susceptibility associated with dinuclear Dy^{III} metal complexes, the magnetic properties of **1**·4C$_6$H$_6$ and **2** were investigated using a SQUID magnetometer. The direct current (dc) susceptibility data obtained at 1000 Oe display room temperature χT products of 27.83 cm^3 K mol^{-1} and 27.53 cm^3 K mol^{-1} for **1**·4C$_6$H$_6$ and **2**, respectively (Fig. 3). These values are in good agreement with the theoretical χT values estimated for two non-interacting Dy^{III} ions (S= 5/2; L=5; $^6H_{15/2}$; g= 4/3; χT_{RT}= 14.17 cm^3 K mol^{-1}). The similarities between the room temperature values for both compounds further support the absence of any additional spins (i.e., radical ligands) within **2**, corroborating the self-association of the bpytz$^{\bullet-}$ ligands and the resulting pancake bond formation. In the temperature range of 300 – 100 K, the χT product for both metal complexes remain constant, indicative of the uncoupled nature of the Dy^{III} – Dy^{III} interaction within the molecules. Below 100 K, the decrease of the χT product can be associated with depopulation of the Stark sublevels, spin-orbit coupling and/or weak interactions between the metal ions. Upon comparing the magnetic susceptibility of **1**·4C$_6$H$_6$ *vs.* **2**, the χT product of **2** deviates from linearity at a higher temperature (100 K) than for **1**·4C$_6$H$_6$ (50 K). Fitting of the data using the Lines model[23] affords exchange coupling constants of 0.006 cm^{-1} and 0.016 cm^{-1} for **1**·4C$_6$H$_6$ and **2**, respectively, indicating a weak exchange interaction between the Dy^{III} ions.[24] The slightly stronger coupling constant observed in **2** is likely due to the shorter intramolecular Dy^{III} – Dy^{III} distance of 7.10(8) Å compared with **1**·4C$_6$H$_6$ (8.01(4) Å). Although weak, this slight variation between compounds may be attributed to the intramolecular π-dimerized bpytz$^{\bullet-}$ bridging ligand. In addition, the field dependence of the magnetization (*Mvs. H*/*T*) data does not exhibit saturation likely due to thermally accessible low-lying excited states even at 1.8 K and 7 T (Fig. S10). The isotherm lines do not fully superimpose, suggesting the presence of magnetic anisotropy inherent to Dy^{III} ions.

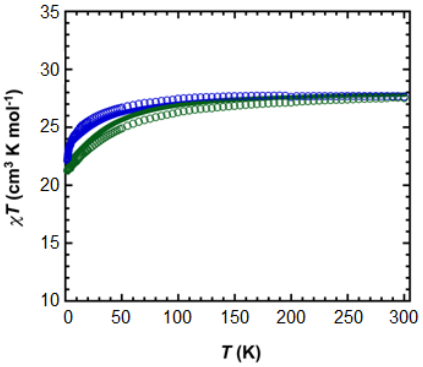

Fig. 3 Variable temperature dc magnetic susceptibility data, where $\chi = M/H$ normalized per mole for **1**·4C$_6$H$_6$ (blue) and **2** (green) obtained under an applied field of 1000 Oe. Experimental data is denoted by circles with the solid line representing the fit.

Owing to the significant spin orbit coupling associated with Dy^{III} ions, such compounds often exhibit a slow relaxation of magnetization, indicative of SMM behaviour. To probe this, dynamic alternating current (ac) susceptibility measurements were performed on **1**·4C$_6$H$_6$ and **2**. At low temperatures and zero dc field, both metal complexes exhibit ac signals; **1**·4C$_6$H$_6$ shows a small tail while **2** displays a slightly pronounced signal (Fig. S11). No clear full peak was observable for either compound under these conditions. This indicates that magnetization relaxation is likely occurring through quantum tunnelling of the magnetization (QTM), thus quenching the SMM behaviour. Nonetheless, upon application of a small static field (1000 Oe), full peaks were observable suggesting that QTM can be minimized and relaxation times can be increased upon application of a field. To further probe the effect of the applied dc field, field dependent measurements were carried out at 2 K with varying magnetic fields up to 1800 Oe for **1**·4C$_6$H$_6$ and 5000 Oe for compound **2** (Fig. S12 and S13). It is noteworthy that two unique "high" and "low" frequency processes can be seen. This data was fit using a generalized/double Debye model for the field dependent ac susceptibility measurements (Tables S12, S13). This data confirms QTM can be minimized and the slow relaxation of the magnetization can be enhanced at 600 Oe for **1**·4C$_6$H$_6$ and 1200 Oe for **2**.

Upon performing temperature dependent (6 to 1.9 K) ac susceptibility measurements in the presence of a static dc field of 600 Oe, frequency dependent out-of-phase signals were observed in **1**·4C$_6$H$_6$, revealing its SMM behaviour (Fig.4 and S14). This data was fit using the generalized Debye model utilizing *CC-FIT2* software,[25] through which the relaxation times (τ) and their respective distributions (α) were extracted (Tables S12-S15 for parameters of best fit for each temperature curve). Given the nature of the SMM behaviour, it is vital to consider not just thermally induced relaxation processes, but also other relaxation mechanisms such as Raman, direct and QTM processes. Upon plotting τ^{-1} *vs.* T on logarithmic axes, a

distinct linear trend can be observed. This is indicative that over the temperature ranges where values of τ can be observed, the dominant mechanism of magnetisation relaxation occurs *via* Raman processes ($\tau^{-1} = CT^n$; eq. (1)). Upon fitting the extracted relaxation times for **1**·4C$_6$H$_6$ using eq. (1), the following parameters were obtained: C = 0.457 s^{-1} K$^{-5.09}$ and n = 5.09. Fits employing terms for Orbach ($\tau^{-1} = \tau_o^{-1} \exp(-U_{eff}/K_B T)$; (eq. (2)) and QTM ($\tau^{-1}_{QTM}$) did not improve the quality of the fit, thus validating the Raman relaxation mode as the primary contributor to the slow relaxation of the magnetisation.

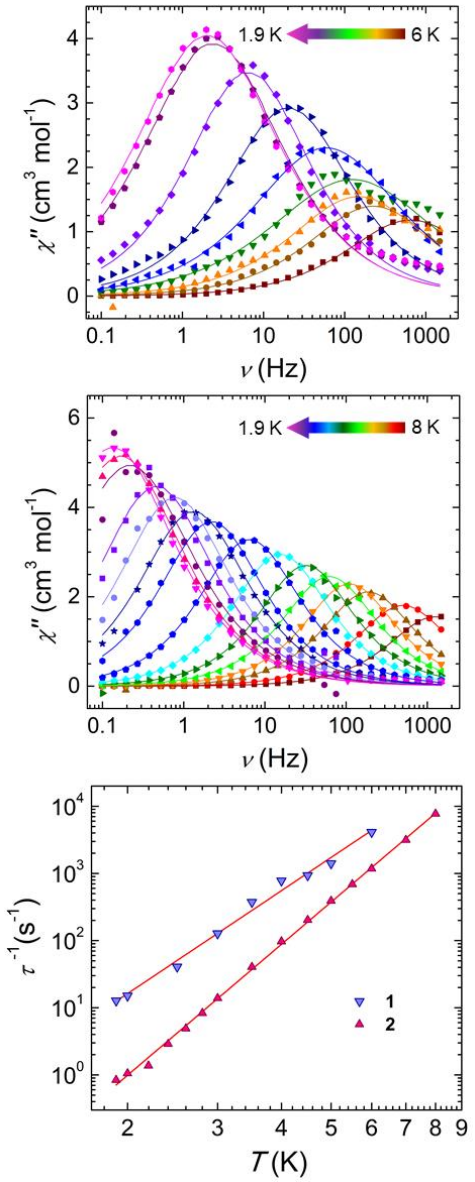

Fig. 4 Frequency dependence of the out-of-phase susceptibility (χ'') at variable temperatures performed at 600 Oe for **1**·4C$_6$H$_6$ (top) and 1200 Oe for **2** (middle). The solid lines represent best fits obtained from the generalized Debye model using *CC-FIT2*. Plot of the τ^{-1} *vs.* T on a log-log scale (bottom) with the fit (red line) using eq. (1).

In the case of **2**, similar frequency dependent signals were observed at 1200 Oe below 8 K, also demonstrating SMM behaviour (Fig. 4, middle). Using the same approach as **1**·4C$_6$H$_6$, the data was fit utilizing the generalized Debye model in *CC-FIT2*, and the relaxation times and distributions were extracted.[25] The data was further fit using a Raman model (eq. (1)), through which the following parameters were obtained: C = 0.011 s^{-1} K$^{-6.48}$ and n = 6.48. Similar to **1**·4C$_6$H$_6$, adding Orbach or QTM terms did not improve the quality of the fit and did not yield physically reasonable values further supporting a Raman process as the dominant magnetisation relaxation mechanism.

In light of the above results, the magnetic properties of the centrosymmetric compounds **1**·4C$_6$H$_6$ and **2** arise mainly from two non-interacting Dy^{III} ions. This may be attributed to the shielded core 4*f* magnetic orbitals of Dy^{III} ions along with the diamagnetic bridging ligand(s) that link the metal centres in both metal complexes. To investigate the magnetic properties of **1**·4C$_6$H$_6$ and **2** in more detail, the standard CASSCF/SO-RASSI calculations[13] followed by SINGLE_ANISO[26] and POLY_ANISO[27] routines were performed (see ESI for details). The CASSCF/SO-RASSI calculations revealed that the principle magnetic axes of the ground Kramers doublet (KD) are oriented to 91° and 86° angle with respect to the line connecting two Dy^{III} ions in **1** and **2**, respectively (Fig. S15). In both compounds, the angles between the magnetic axes of the ground and excited doublets vary significantly from ~16° to 170°, neither of which are colinear to the main magnetic axes of the ground KD (Tables S16 and S17). Close inspection of the ***g***-tensor of the ground KD (**1**: g_x = 0.048, g_y = 0.084, g_z = 19.376; **2**: g_x = 0.035, g_y = 0.037, g_z = 18.667), shows non-negligible transverse components in both molecules, as they deviate from the ideal values of highly axial ***g***-tensors ($g_x = g_y = 0.0$, $g_z \approx 20.0$). This likely leads to the mixing of the ground state with the higher excited state, thus promoting significant QTM as observed experimentally. More specifically, the percentage composition of the SO-RASSI wavefunctions of the sixteen lowest states are presented in Tables S18 and S19 for **1** and **2**, respectively. As can be seen, the ground doublet within **1** is mainly composed of M_J = ±15/2 states, which is common for Dy^{III} SMMs.[28] The higher lying doublets of **1** are considerably more mixed than the ground doublet and cannot be uniquely defined by a single M_J state. The ground doublet of **2** is not pure M_J = ±15/2 state but contains mixing from M_J = ±13/2 (4 %) and M_J = ±11/2 states (12 %), as well as smaller contributions from several higher lying states. As expected, the higher lying doublets are strongly mixed within **2**. Taking into account all the above-mentioned data, it can be concluded that the low symmetry environment of the Dy^{III} ions effectively diminishes the axiality of KDs and leads to the strong mixing of states in both metal complexes.

The low axial ***g***-tensors of the ground KDs, as well as the weak exchange interaction between the metal centres, usually promotes QTM within the ground KD.[24] To further study the relaxation of magnetisation in both compounds, the qualitive energy barrier for both were constructed by plotting the energies of the lowest lying states with respect to their magnetic moments and calculating the transition magnetic moment matrix elements between the states, i.e., transition probabilities (Fig. S16).[26c] The calculated transition probabilities for both metal complexes show a rather large value for a matrix element

connecting the two components of the ground KD: for **1** the value is 0.022, whereas for **2** it is 0.012. Such high values are usually associated with efficient QTM within the ground KD.[24a] The computational result is fully in line with experimental findings; **1**·4C_6H_6 and **2** show the relaxation of magnetisation only when the degeneracy of the ground KDs are lifted with the application of external dc field.

In conclusion, we report two new tetrazine bridged dinuclear Dy^{III} metal complexes exhibiting SMM behaviour revealed through an applied dc field. In **2**, which contains two reduced tetrazine moieties, a unique coordination induced π-dimer connecting the two metal centres is observed. This represents the first example of an unusual intramolecular pancake bond, which is supported experimentally and through computational studies. More specifically, the similarity of the χT products for **1**·4C_6H_6 and **2**, as well as the calculated vertical (~-3250 to -4000 cm^{-1}) and adiabatic (~-1780 to -2600 cm^{-1}) radical-radical coupling constants ($J_{rad\text{-}rad}$), along with the EPR studies suggest that the two tetrazine rings are strongly antiferromagnetically coupled in **2**, which makes the $(bpytz^{\bullet-})_2$ bridge a diamagnetic linker between two Dy^{III} ions. Under an applied field of 600 Oe for **1**·4C_6H_6 and 1200 Oe for **2**, both compounds exhibit slow relaxation of the magnetisation occurring *via* Raman process. The results found in this ongoing project will be helpful for future strategies on designing new lanthanide metal complexes containing tetrazinyl-based radicals in the pursuit to exploit direct exchange coupling.

We thank the University of Ottawa, the CFI, the NSERC and the Academy of Finland (projects 315829, 320015) for their financial support. M. A. L. thanks Conselho Nacional de Desenvolvimento Científico e Tecnológico (CNPQ; 201395/2014-6) for a PhD scholarship. CSC-IT Centre for Science in Finland, the Finnish Grid and Cloud Infrastructure (persistent identifier urn:nbn:fi:research-infras-2016072533) and Prof. H. M. Tuononen (University of Jyväskylä) are acknowledged for providing computational resources for the project.

References

1 R.G. Hicks, ed., "*Stable Radicals: Fundamentals and Applied Aspects of Odd-Electron Compounds*", John Wiley & Sons, Ltd.: Wiltshire, 2010

2 (a) X. Ma, E. A Suturina, M. Rouzieres, M. Platunov, F. Wilhelm, A. Rogalev, R. Clérac, P. Dechambenoit, Using redox-active π bridging ligand as a control switch of intramolecular magnetic interactions, *J. Am. Chem. Soc*., 2019, **141**, 7721-7725; (b) E. M. Fatila, M. Rouziere, M. C. Jennings, A. J. Lough, R. Clerac, K. E. Preuss, Fine-tuning the single-molecule magnet properties of a [Dy(III)-radical]$_2$ pair, *J. Am. Chem. Soc*., 2013, **135**, 9596-9599; (c) S. Fortier, J. J. Le Roy, C.-H. Chen, V. Vieru, M. Murugesu, L. F. Chiboratu, D. J. Mindiola, K. G. Caulton, A dinuclear cobalt complex featuring unprecedented anodic and cathodic redox switches for single-molecule magnet activity, *J. Am. Chem. Soc*., 2013, **135**, 14670-14678; (d) D. I. Alexandropoulos, B. S. Dolinar, K. R. Vignesh, K. R. Dunbar, Putting a new spin on supramolecular metallacycles: Co_3 triangle and Co_4 square bearing tetrazine-based radicals as bridges, *J. Am. Chem. Soc*., 2017, **139**, 11040-11043; (e) J. A. DeGayner, I.-R. Jeon, T. D. Harris, A series of tetraazalene radical bridged M_2 (M = Cr^{III}, Mn^{II}, Fe^{II}, Co^{II}) complexes with strong magnetic exchange coupling, *Chem. Sci*., 2015, **6**, 6639-6648.

3 (a) J. D. Rinehart, M. Fang, W. J. Evans, J. R. Long, A N_2^{3-} radical-bridged terbium complex exhibiting magnetic hysteresis at 14 K, *J. Am. Chem. Soc*., 2011, **133**, 14236-14239; (b) S. Demir, I.-R. Jeon, J. R. Long, T. D. Harris, Radical ligand-containing single-molecule magnets, *Coord. Chem. Rev*., 2015, **289**, 149-176; (c) S. Demir, M. I. Gonzalez, L. E. Darago, W. J. Evans, J. R. Long, Giant coercivity and high magnetic blocking temperatures for N_2^{3-} radical bridged dilanthanide complexes upon ligand dissociation, *Nature Commun*., 2017, **8**, 2144; (d) B. S. Dolinar, D. I. Alexandropoulos, K. R. Vignesh, T. James, K. R. Dunbar, Lanthanide triangles supported by radical bridging ligands, *J. Am. Chem. Soc*., 2018, **140**, 908-911 (e) H. Miao, M. Li, H.-Q. Li, F.-X. Shen, Y.-Q. Zhang, X.-Y. Wang, Syntheses and magnetic properties of a bis-tridentate nitronyl nitroxide radical and its metal complexes, *Dalton Trans*., 2019, **48**, 4774-4778; (f) Z.-X. Xiao, H. Miao, D. Shao, H.-Y. Wei, Y.-Q. Zhang, X.-Y. Wang, Single-molecule magnet behaviour in a dysprosium-triradical complex, *Chem. Commum*., 2018, **54**, 9726-9729; (g) I.-R. Jeon, J. G. Park, D. J. Xiao, T. D. Harris, An azophenine radical-bridged Fe_2 single-molecule magnet with record magnetic exchange coupling, *J. Am. Chem. Soc*., 2013, **135**, 16845-16848.

4 (a) F.-S. Guo, B. M. Day, Y.-C. Chen, M.-L. Tong, A. Mansikkamäki, R. A. Layfield, Magnetic hysteresis up to 80 kelvin in a dysprosium metallocene single-molecule magnet, *Science*, 2018, **362**, 1400-14003; (b) C. A. P. Goodwin, F. Ortu, D. Reta, N. F. Chilton, D. P. Mills, Molecular magnetic hysteresis at 60 kelvin in dysprosocenium, *Nature*, 2017, **548**, 439-442; (c) G. Christou, D. Gatteschi, D. N. Hendrickson, R. Sessoli, Single-molecule magnets, *MRS Bull.* 2000, **25**, 66-71; (d) S.-D. Jiang, B.-W. Wang, H.-L. Sun, Z.-M. Wang, S. Gao, An organometallic single-ion magnet, *J. Am. Chem. Soc*., 2011, **133**, 4730-4733. (e) K. L. M. Harriman, M. Murugesu, An organolanthanide building block approach to single-molecule magnets, *Acc. Chem. Res.*, 2016, **49**, 1158-1167.

5 (a) T. J. Woods, M. F. Ballesteros-Rivas, S. M. Ostrovsky, A. V. Palii, O. S. Reu, S. I. Klokishner, K. R. Dunbar, Strong direct magnetic coupling in a dinuclear Co^{II} tetrazine radical single-molecule magnet, *Chem. Eur. J.*, 2015, **21**, 10302-10305; (b) M. A. Lemes, G. Brunet, A. Pialat, L. Ungur, I. Korobkov, M. Murugesu, Strong ferromagnetic exchange coupling in a {Ni^{II}_4} cluster mediated through an air-stable tetrazine-based radical anion, *Chem. Commun*, 2017, **53**, 8660-8663; (c) T. J. Woods, H. D. Stout, B. S. Dolinar, K. R. Vignesh, M. F. Ballesteros-Rivas, C. Achim, K. Dunbar, Strong ferromagnetic exchange coupling mediated by a bridging tetrazine radical in a dinuclear nickel complex, *Inorg. Chem*. 2017, **56**, 12094-12097; (d) M. Schwach, H. D. Hausen, W. Kaim, The first crystal structure of a metal-stabilized tetrazine anion radical: formations of a dicopper complex through self-assembly in a comproportionation reaction, *Inorg. Chem.*, 1999, **38**, 2242-2243; (e) M. Glockle, K. Hubler, H. J. Kummerer, G. Denninger, W. Kaim,Dicopper (I) complexes with reduced states of 3,6-bis(2'-pyrimidyl)-1,2,4,5-tetrazine: crystal structures and spectroscopic properties of the free ligand, a radical species, and a complex of the 1,4-dihydro form, *Inorg. Chem.*, 2001, **40**, 2263-2269; (f) K. Parimal, S. Vyas, C. H. Chen, C. M. Hadad, A. H. Flood, Bond elongation in the anion radical of coordicated tetrazine ligands: a crystallographic, spectroscopic and computational study of a reduced {$Re(CO)_3Cl$} complex, *Inorg. Chim. Acta*, 2011, **374**, 620-626; (g) S. K. Tripathy, M. van der Meer, A. Sahoo, P. Laha,

N. Dehury, S. Plebst, B. Sarkar, K. Samanta, S. Patra, A dinuclear [{(*p*-cym)$Ru^{II}Cl$}$_2$(μ-bpytz$^{\bullet-}$)]$^+$ complex bridged by a radical anion: synthesis, spectrochemical, EPR and theoretical investigation (bpytz = 3,6-bis(3,5-dimethylpyrazolyl)1,2,4,5-tetrazine; *p*-cym = *p*-cymene), *Dalton Trans.*, 2016, **45**, 12532-12538; (h) M. A. Lemes, H. N. Stein, B. Gabidullin, K. Robeyns, R. Clérac, M. Murugesu, Probing magnetic-exchange coupling in supramolecular squares based on reducible tetrazine-derived ligands, *Chem. Eur. J.*, 2018, **24**, 4259-4263; (i) W. Kaim, The coordination chemistry of 1,2,4,5-tetrazines, *Coord. Chem. Rev.*, 2002, **230**, 127-139; (j) G. Brunet, M. Hamwi, M. A. Lemes, B. Gabidullin, M. Murugesu, A tunable lanthanide cubane platform incorporating air-stable radical ligands for enhanced magnetic communication, *Commun. Chem*. 2018, **1**, 88.

6 B. D. Koivisto, A. S. Ichimura, R. McDonald, M. T. Lemaire, L. K. Thompson, R. G. Hicks, Intramolecular π-dimerization in a 1,1′-bis(verdazyl)ferrocene diradical, *J. Am. Chem. Soc.*, 2006, **128**, 690-691.

7 D. Casanova, M. Llunell, P. Alemany, S. Alvarez, The rich stereochemistry of eight-vertex polyhedra: a continuous shape measures study, *Chem. Eur. J*., 2005, **11**, 1479-1494.

8 A. Bondi, van der Waals volumes and radii, *J. Phys. Chem.*, 1964, **68**, 441-451.

9 (a) J. Miller, J. J. Novoa, Four-center carbon-carbon bonding,*Acc. Chem. Res.*, 2007, **40**, 189-196; (b) H. Endres, in *Extended Linear Chain Compounds*, ed. J.S. Miller, Plenum Press. New York, 1983, vol. 3, ch. 5, 263-317.

10 (a) D. Gut, A. Rudi, J. Kopilov, I. Goldberg, M. Kol, Pairing of propellers: dimerization of octahedral ruthenium(II) and osmium(II) complexes of eilatin via π-π stacking featuring heterochiral recognition,*J. Am. Chem. Soc.*, 2002, **124**, 5449-5456; (b) J. Yuasa, T. Suenobu, S. Fukuzumi, Highly self-organized electron transfer from an iridium complex to *p*-benzoquinone due to formation of a π-dimer radical anion complex triply bridged by scandium ions,*J. Am. Chem. Soc.*, 2003, **125**, 12090-12091.

11 K. E. Preuss, Pancake bonds: π-stacked dimers of organic and light-atom radicals, *Polyhedron*, 2014, **79**, 1-15.

12 (a) L. Noodleman, Valence bond description of antiferromangetic coupling in transition metal dimers, *J. Chem. Phys.*, 1981, **74**, 5737. (b) L. Noodleman, E. R. Davidson, Ligand spin polarization and antiferromagnetic coupling in transition metal dimers, *Chem. Phys.*, 1986, **109**, 131-143; (c) L. Noodleman, J. G. Norman, J. H. Osborne, A. Aizman, D. A. Case, Models for ferredoxins: electronic structures of iron-sulfur clusters with one, two, and four iron atoms, *J. Am. Chem. Soc.*, 1985, **107**, 3418-3426; (d) W. Koch, M. C. Holthausen, *A Chemist's Guide to Density Functional Theory*, Wiley-VCH Verlag GmbH, Weinheim, FRG, 2001. (e) M. Kertesz, Pancake bonding: an unusual pi-stacking interaction, *Chem. Eur. J*., 2019, **25**, 400-416

13 (a) P. Siegbahn, A. Heiberg, B. Roos, B. Levy, A comparison of the super-CI and the Newton-Raphson scheme in the complete active space SCF method, *Phys. Scr*., 1980, **21**, 323-327; (b) B. O. Roos, P. R. Taylor, P. E. M. Sigbahn, A complete active space SCF method using a density matrix formulated super-CI approach, *Chem. Phys.*, 1980, **48**, 157-173; (c) B. O. Roos, R. Lindh, P. Å. Malmqvist, V. Veryazov and P.-O. Widmark, *Multiconfigurational Quantum Chemistry*, John Wiley & Sons, Inc., Hoboken, NJ, USA, 2016.

14 (a) A. Mansikkamäki, H. M. Tuononen, The role of orbital symmetries in enforcing ferromagnetic ground state in mixed radical dimers, *J. Phys. Chem. Lett.*, 2018, **9**, 3624-3630; (b) D. Reta Mañeru, A. K. Pal, I. de P. R. Moreira, S. N. Datta, F. Illas, The triplet-singlet gap in the *m*-xylylene radical: a not so simple one, *J. Chem. Theory Comput*., 2014, **10**, 335-345.

15 J. Gräfenstein, E. Kraka, M. Filatov and D. Cremer, Can Unrestricted Density-Functional Theory Describe Open Shell Singlet Biradicals?, *Int. J. Mol. Sci.*, 2002, **3**, 360.

16 (a) K. Yamaguchi, T. Tsunekawa, Y. Toyoda and T. Fueno, Ab initio molecular orbital calculations of effective exchange integrals between transition metal ions,*Chem. Phys. Lett.*, 1988, **143**, 371. (b) K. Yamaguchi, H. Fukui and T. Fueno, Molecular orbital (MO) theory for magnetically interacting organic compounds. Ab-initio MO calculations of the effective exchange integrals for cyclophane-type carbene dimers, *Chem. Lett.*, 1986, **15**, 625. (c) K. Yamaguchi, F. Jensen, A. Dorigo and K. N. Houk, A spin correction procedure for unrestricted Hartree-Fock and Møller-Plesset wavefunctions for singlet diradicals and polyradicals, *Chem. Phys. Lett.*, 1988, **149**, 537.

17 (a) O. A. Vydrov and G. E. Scuseria, Assessment of a long-range corrected hybrid functional, *J. Chem. Phys*., 2006, **125**, 234109. (b) O. A. Vydrov, J. Heyd, A. V. Krukau and G. E. Scuseria, Importance of short-range versus long-range Hartree-Fock exchange for the performance of hybrid density functionals, *J. Chem. Phys*., 2006, **125**, 074106. (c) O. A. Vydrov, G. E. Scuseria and J. P. Perdew, Tests of functionals for systems with fractional electron number, *J. Chem. Phys*., 2007, **126**, 154109. (d) C. Lee, W. Yang and R. G. Parr, Development of the Colle-Salvetti correlation-energy formula into a functional of the electron density,*Phys. Rev. B*, 1988, **37**, 785. (e) A. D. Becke, Density-functional thermochemistry. III. The role of exact exchange, *J. Chem. Phys*., 1993, **98**, 5648. (f) A. D. Becke,Density-functional exchange-energy approximation with correct asymptotic behavior, *Phys. Rev. A*, 1988, **38**, 3098. (g) M. Ernzerhof and G. E. Scuseria, Assessment of the Perdew-Burke-Ernzerhof exchange-correlation functional, *J. Chem. Phys*., 1999, **110**, 5029. (h) C. Adamo and V. Barone, Toward reliable density functional methods without adjustable parameters: The PBE0 model, *J. Chem. Phys.*, 1999, **110**, 6158.

18 (a) F. Weigend and R. Ahlrichs, Balanced basis sets of split valence, triple zeta valence and quadruple zeta valence quality for H to Rn: Design and assessment of accuracy, *Phys. Chem. Chem. Phys.*, 2005, **7**, 3297. (b) D. Andrae, U. Häußermann, M. Dolg, H. Stoll and H. Preuß, Energy-adjusted *ab initio* pseudopotentials for the second and third row transition elements, *Theor. Chim. Acta*, 1990, **77**, 123. (c) S. Grimme, J. Antony, S. Ehrlich and H. Krieg, A consistent and accurate *ab initio* parametrization of density functional dispersion correction (DFT-D) for the 94 elements H-Pu,*J. Chem. Phys*., 2010, **132**, 154104. (d) S. Grimme, S. Ehrlich and L. Goerigk, Effect of the damping function in dispersion corrected density functional theory, *J. Comput. Chem*., 2011, **32**, 1456.

19 (a) M. Head-Gordon, Characterizing unpaired electrons from the one-particle density matrix, *Chem. Phys. Lett.*, 2003, **372**, 508. (b) M. Head-Gordon, Reply to comment on 'characterizing unpaired electrons from the one-particle matrix', *Chem. Phys. Lett.*, 2003, **380**, 488.

20 Z. Cui, H. Lischka, H. Z. Beneberu and M. Kertesz, Double Pancake Bonds: Pushing the Limits of Strong π-π Stacking Interactions, *J. Am. Chem. Soc.*, 2014, **136**, 12958.

21 M. S. Gordon, M. W. Schmidt, G. M. Chaban, K. R. Glaesemann, W. J. Stevens and C. Gonzalez, A natural orbital diagnostic for multiconfigurational character in correlated wave functions, *J. Chem. Phys.*, 1999, **110**, 4199.

22 (a) H. Z. Beneberu, Y.-H. Tian and M. Kertesz, Bonds or not bonds? Pancake bonding in 1,2,3,5-dithiadiazolyl and 1,2,3,5-diselenadiazolyl radical dimers and their derivatives, *Phys. Chem. Chem. Phys.*, 2012, **14**, 10713. (b) Z. Cui, H. Lischka,

T. Mueller, F. Plasser and M. Kertesz, Study of the Diradicaloid Character in a Prototypical Pancake-Bonded Dimer: The Stacked Tetracyanoethylene (TCNE) Anion Dimer and the Neutral K_2TCNE_2 Complex, *ChemPhysChem*, 2014, **15**, 165.

23 M. E. Lines, Orbital Angular Momentum in the Theory of Paramagnetic Clusters, *J. Chem. Phys.*, 1971, **55**, 2977.

24 (a) B. S. Dolinar, D. I. Alexandropoulos, K. R. Vignesh, T. James and K. R. Dunbar, Lanthanide Triangles Supported by Radical Bridging Ligands, *J. Am. Chem. Soc.*, 2018, **140**, 908–911. (b) J. O. Moilanen, A. Mansikkamäki, M. Lahtinen, F.-S. Guo, E. Kalenius, R. A. Layfield and L. F. Chibotaru, Thermal expansion and magnetic properties of benzoquinone-bridged dinuclear rare-earth complexes, *Dalton Trans.*, 2017, **46**, 13582.

25 D. Reta and N. F. Chilton, Uncertainty estimates for magnetic relaxation times and magnetic relaxation parameters, *Phys. Chem. Chem. Phys.*, 2019, **21**, 23567.

26 (a) L. F. Chibotaru and L. Ungur, *Ab initio* calculation of anisotropic magnetic properties of complexes. I. Unique definition of pseudospin Hamiltonians and their derivatives, *J. Chem. Phys.*, 2012, **137**, 064112. (b) L. Ungur and L. F. Chibotaru, Ab Initio Crystal Field for Lanthanides, *Chem.Eur. J.*, 2017, **23**, 3708. (c) L. Ungur, M. Thewissen, J.-P. Costes, W. Wernsdorfer and L. F. Chibotaru, Interplay of Strongly Anisotropic Metal Ions in Magnetic Blocking of Complexes, *Inorg. Chem.*, 2013, **52**, 6328.

27 (a) L. F. Chibotaru, L. Ungur and A. Soncini, The Origin of Nonmagnetic Kramers Doublets in the Ground State of Dysprosium Triangles: Evidence for a Toroidal Magnetic Moment, *Angew. Chemie Int. Ed.*, 2008, **47**, 4126. (b) L. Ungur, W. Van den Heuvel and L. F. Chibotaru, *Ab initio* investigation of the non-collinear magnetic structure and the lowest magnetic excitations in dysprosium triangles, *New J. Chem.*, 2009, **33**, 1224.

28 (a) F.-S. Guo, B. M. Day, Y.-C. Chen, M.-L. Tong, A. Mansikkamäki and R. A. Layfield, A Dysprosium Metallocene Single-Molecule Magnet Functioning at the Axial Limit, *Angew. Chem., Int. Ed*., 2017, **56**, 11445; (b) S. Jiang, B. Wang, H. Sun, Z. Wang and S. Gao, An Organometallic Single-Ion Magnet, *J. Am. Chem. Soc*., 2011, **133**, 4730; (c) Y.-S. Meng, Y.-Q. Zhang, Z.-M. Wang, B.-W. Wang and S. Gao, Weak Ligand-Field Effect from Ancillary Ligands on Enhancing Single-Ion Magnet Performance, *Chem. – Eur. J*., 2016, **22**, 12724; (d) C. A. P. Goodwin, F. Ortu, D. Reta, N. F. Chilton and D. P. Mills, Molecular magnetic hysteresis at 60 kelvin in dysprosocenium, *Nature*, 2017, **548**, 439; (e) C. P. Burns, B. O. Wilkins, C. M. Dickie, T. P. Latendresse, L. Vernier, K. R. Vignesh, N. S. Bhuvanesh and M. Nippe, A comparative study of magnetization dynamics in dinuclear dysprosium complexes featuring bridging chloride or trifluoromethanesulfonate ligands, *Chem. Commun.*, **2017**, 53, 8419. (f) F.-S. Guo, B. M. Day, Y.-C. Chen, M.-L. Tong, A. Mansikkamäki and R. A. Layfield, Magnetic hysteresis up to 80 kelvin in a dysprosium metallocene single-molecule magnet, *Science*, 2018, **362**, 1400.